



The effect of the thickness of the adhesive layer on the ballistic limit of ceramic/metal armours. An experimental and numerical study

J. López-Puente, A. Arias, R. Zaera, C. Navarro*

Department of Continuum Mechanics and Structural Analysis, Carlos III University of Madrid Avda. de la Universidad 30, 28911 Leganés, Madrid, Spain

Abstract

In this work, a study has been made of the effect of the adhesive layer thickness on the efficiency of alumina/aluminium armours. Full-scale tests were made shooting armour piercing projectile against panels thick enough to arrest the projectile and also close to the ballistic limit. The adhesive layer, of different thickness, was of the toughened epoxy resin. The fire tests revealed the influence of thickness on the response of the lightweight protection. Numerical simulations were performed to analyse the experimental results. The analysis showed an optimum adhesive layer thickness for the best performance of the lightweight protection considered.

Keywords: Adhesive; Ceramic; Lightweight armours; Impact

1. Introduction

The protection of solids against high velocity impacts (above 500 m/s) has been studied intensively in the last decades. The use of ballistic projectiles with cores of greater hardness called for more efficient armours, introducing new materials and new protection systems. This

*Corresponding author. Fax: +34 91 624 94 30.

E-mail address: navarro@ing.uc3m.es (C. Navarro).

development has been remarkable in lightweight armours in which weight is a key factor if the target is mobile (vehicles, aircraft, security corps). The fuel cost of civil or military vehicles and planes increases if heavy protective panels are added to the structure; the mobility of security and defence corps decreases if the personnel wear heavy jackets or helmets. Dual hardness panels have shown improved efficiency over monolithic metallic armours [1] since the hard layer, which firstly receives the impact, serves to erode the core of the projectile, while the softer layer absorbs its kinetic energy. Foremost among the various types of dual hardness armours are those with tiles of advanced ceramic as the hard layer and aluminium alloys or steel as the backing plate; the ceramic tiles being bonded to the rear plate by an adhesive layer (Fig. 1). Fibre-reinforced polymers could also be used for the rear plate for better efficiency, but metal have the double advantage of being cheaper than fibre laminates and of serving the structural as well as the protective function. On comparing the weight of conventional steel armour plating (Rolled Homogeneous Armour of 60 Rockwell C hardness) with that of ceramic armours, it is found that the latter are up to 65% lighter if carbides, nitrides or borides are used as the hard layer (Fig. 2), but the higher cost of these ceramics counter-balances the use of alumina for armour applications, except for personal protection or in the design of systems in which the weight is of prime importance.

The behaviour of ceramic/metal panels against impact may be determined by deterministic or by probabilistic techniques [2]. In the former, numerical codes or simplified engineering models are used to simulate the impact problem. In the other approach, experimental data can provide a probability of perforation curve (Fig. 3) of which each region is related to one of the situations depicted in Fig. 4. In this Fig. “A” corresponds to projectile arrest, “C” to target perforation and “B” to the range of impact velocities at which perforation is probable. The critical impact velocity at which the probability of perforation is $P\%$ is known as *ballistic limit* v_P .

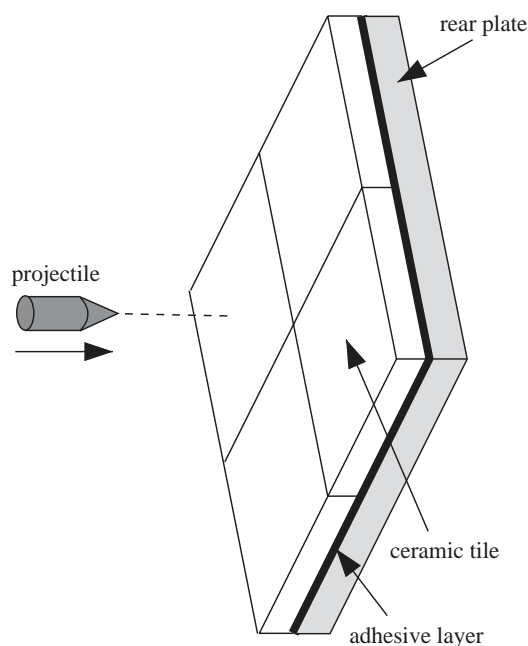


Fig. 1. Layout of a ceramic lightweight armour.

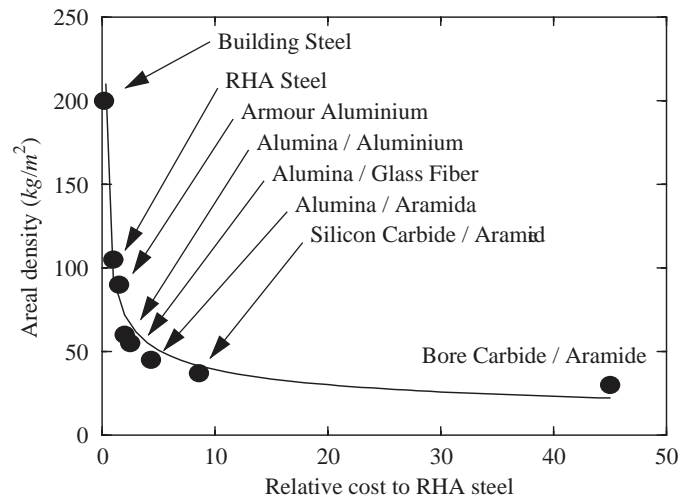


Fig. 2. Areal density needed to arrest 7.62 AP projectile at 800 m/s vs. armour cost [11].

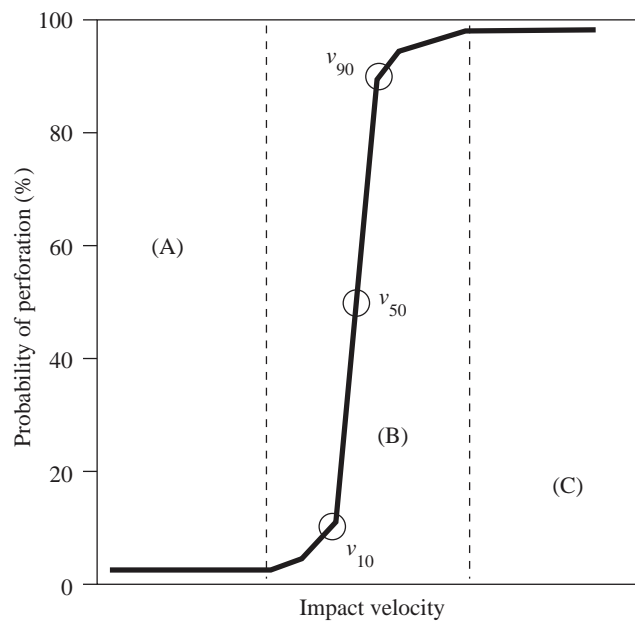


Fig. 3. Probability of perforation vs. impact velocity.

Some workers have shown the influence of the adhesive layer in the ballistic behaviour of the armour when perforation takes place. Full-scale fire tests performed by Marshall [3] evidenced that the residual velocity of the projectile after perforation may be influenced by the adhesive type that joins the ceramic to the rear plate. James [4] studied the influence of the mechanical impedance of the adhesive on the behaviour of the armour. A more detailed study is found in [5] in which the effect of the type and of the thickness of the adhesive layer are considered for add-on armours, which diminish the kinetic energy of the projectile before it impacts on the main armour.

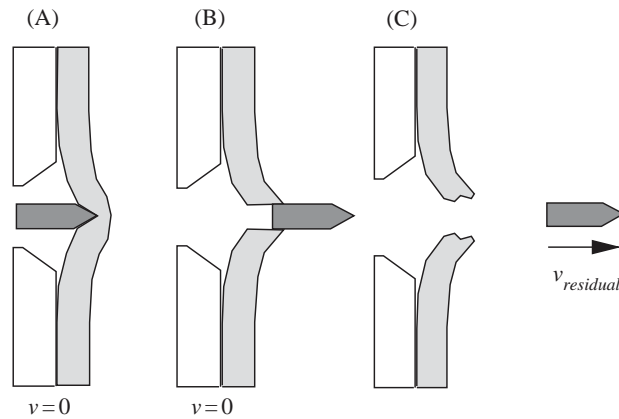


Fig. 4. Different final situations after impact: Arrest (A), Ballistic Limit (B) and Perforation (C).

However, this effect must also be studied in the other two regions; in some applications, such as personnel armouring, the degree of protection must be complete and no penetration must occur; even the projection of debris to the rear side or an excessive deflection of the panel must be avoided. The effect of the adhesive layer on the velocity below which no perforation occurs, is also of great interest.

Here we study the effect of the adhesive *thickness* on the efficiency of alumina/aluminium armours in regions “A” (projectile arrest) and “B” (ballistic limit). Ballistic tests and numerical simulations allowed a description of the interaction between ceramic tile and metallic backing plate through this polymeric layer and revealed the existence of an optimum value in the adhesive layer thickness for the best performance of the lightweight protection.

2. Experimental tests

A set of fire tests were carried out with *Morgan Matroc* 98% purity alumina tiles bonded to the aluminium *2017-T6* backing plate with a *Hysol EA-9361* toughened epoxy resin. Two different armour configurations were analyzed; their geometry was selected to give similar values of areal density with different alumina and aluminium thicknesses in order to get performances just below or above perforation conditions (Table 1). The ceramic tiles, of $100 \times 100 \text{ mm}^2$ in configuration I and $51 \times 51 \text{ mm}^2$ in configuration II, were enclosed in a frame of *SAE 4130 steel* to reproduce a tile-array configuration.

For each type of configuration, three different thicknesses of adhesive were applied: 0.1, 0.5 and 1.1 mm. The armours were impacted using a 7.62 AP projectile with a 5.9 g tungsten carbide core and length/diameter = 3.6 (Fig. 5) launched at 940 m/s. Twenty four valid tests were carried out, i.e., four tests of each configuration and thickness of the adhesive layer, considering valid those in which the projectile impacted correctly at the center of the target.

After the test the deformation of the metallic plate was measured. Detached from the ceramic, the plate was cut transversally with a diamond thread at low speed to avoid mechanical damage. Each cross section (Fig. 6) was photographed with a high-resolution camera and the images were digitalized to obtain the average profile for each configuration and for each adhesive thickness.

Table 1
Armour configurations considered

Configuration	Al thickness (mm)	Al ₂ O ₃ thickness (mm)	Areal density (kg/m ²)
I	6.0	12.0	61.1
II	12.0	8.3	63.4

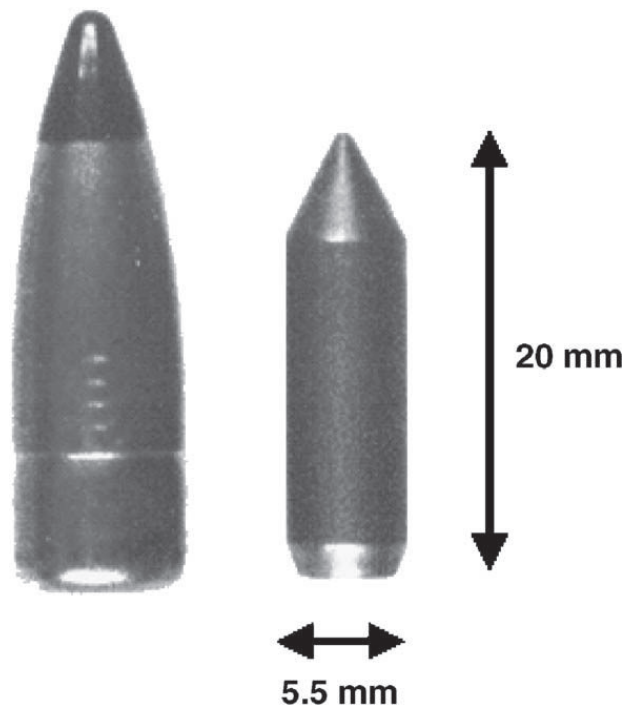


Fig. 5. 7.62 AP projectile and its core.

3. Numerical simulation

For the numerical simulation we used the commercial finite difference computer code AUTODYN-2D [6], specifically developed for problems involving high strain rates. A Lagrangian mesh with axial symmetry was used for all the solids; projectile, ceramic tile, adhesive layer and backing plate.

3.1. Material modelling

Different strength models and state equations were used for the materials of the solids involved in the impact process. For the aluminium and the epoxy resin AUTODYN-2D material libraries were used, while the mechanical behaviour of tungsten carbide and alumina were described through a user subroutine.

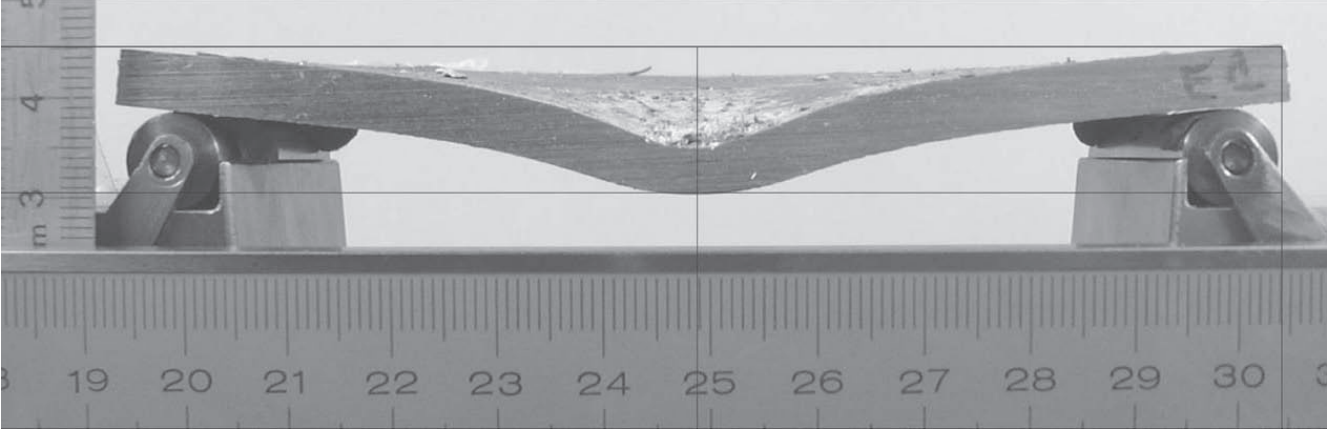


Fig. 6. Cross section of the aluminium backing plate after impact.

3.1.1. Aluminium

For the 2017-*T6* aluminium back-plate, the Steinberg Guinan strength model [7] was used. Often adopted for ductile metallic solids subjected to high strain rates, this model assumes that the shear modulus G rises with pressure and diminishes with temperature according to the expression:

$$G = G_0 \left\{ 1 + \left(\frac{G'_p}{G_0} \right) \frac{p}{\kappa^{1/2}} + \left(\frac{G'_T}{G_0} \right) (T - T_0) \right\}, \quad (1)$$

where G_0 and T_0 are the reference shear modulus and temperature, G'_p and G'_T are material constants (G'_T being negative), p is the pressure, T the temperature, and κ the compression ρ/ρ_0 . This model also considers the variation of the yield stress Y with pressure, temperature and effective plastic strain ε^p according to:

$$Y = Y_0 \left\{ 1 + \left(\frac{Y'_p}{Y_0} \right) \frac{p}{\kappa^{1/2}} + \left(\frac{Y'_T}{Y_0} \right) (T - T_0) (1 + \beta \varepsilon^p)^n \right\}, \quad (2)$$

and subjected to the following restriction:

$$Y_0 (1 + \beta \varepsilon^p)^n \leq Y_{\max}, \quad (3)$$

where Y_0 is the reference yield stress and Y'_p , β and n are material constants. For this material, a Mie Gruneisen equation of state was adopted, relating pressure, specific volume $v = 1/\rho$ and the internal energy e :

$$p = p_r(v) + \frac{\Gamma}{v} [e - e_r(v)], \quad (4)$$

where Γ is the Gruneisen gamma defined as

$$\Gamma = \frac{\Gamma_0}{\kappa}, \quad (5)$$

Γ_0 being a reference value, and p_r and e_r are pressure and energy along the Hugoniot, which is used as the reference curve. Assuming a linear relationship between shock wave velocity U and

Table 2

Aluminium and epoxy parameters for the Steinberg–Guinan model and the Mie–Gruneisen EOS

Material parameter	Aluminium 2017-T6	Epoxy Hysol EA 9361
ρ_0 (kg/m ³)	2785	1186
Y_0 (MPa)	290	—
G_0 (GPa)	28	—
Y_{\max} (MPa)	420	—
β (MPa)	125	—
n	0.1	—
G'_T (MPa/K)	−17.6	—
G'_p	1.8	—
Y'_p	1.89×10^{-2}	—
Γ_0	2	1.13
c_0 (m/s)	5328	2730
S	1.338	1.49

particle velocity u_p such as

$$U = c_0 + S u_p, \quad (6)$$

where c_0 is the sound speed velocity, and S is a material constant; the expression for the Hugoniot pressure and energy are given by

$$p_r(v) = \frac{c_0^2 \rho_0 (1 - \rho_0 v)}{(1 + S(\rho_0 v - 1))^2}, \quad (7)$$

$$e_r(v) = \frac{c_0^2 (\rho_0 v - 1)}{2(1 + S(\rho_0 v - 1))^2}. \quad (8)$$

Table 2 shows the parameters adopted for the aluminium.

3.1.2. Epoxy resin

For the *Hysol EA-9361* epoxy adhesive the Mie Gruneisen equation of state was used. Due to its low strength, as compared with that of the other materials, the resin was considered as a fluid resisting high pressures. Table 2 shows the parameters adopted for the epoxy.

3.1.3. Alumina and tungsten carbide

For both kind of materials, the same constitutive model was used with different parameters. The damage model proposed by Cortés et al. [8] was adopted for both the alumina and the tungsten carbide. This model associates the degree of ceramic fragmentation with a damage variable η affecting the yield stress according to the equation:

$$Y = (1 - \eta) Y_i + \eta Y_c, \quad (9)$$

Table 3
Alumina and tungsten carbide parameters for the Cortes et al. model [8]

Material parameter	Alumina 98% purity	Tungsten carbide
ρ_0 (kg/m ³)	3740	15000
K (GPa)	228	500
G (GPa)	150	257
$\dot{\eta}_0$ (Pa ⁻¹)	0.0025	0.00025
p_0 (MPa)	-100	-2500
μ	0.5	0.5
A (MPa)	446.7	2200
B	2.7	1.6

where Y_i takes into account the strength of the intact fraction through a Drucker Prager yield criterion:

$$Y_i = Ap + B, \quad (10)$$

A and B being material constants.

The term Y_c of equation accounts for the fragmented fraction which behaves as a frictional medium according to the Coulomb law:

$$Y_c = \mu p, \quad (11)$$

where μ is the internal friction coefficient.

The evolution of the damage parameter-within the range [0,1]-is specified by the relation:

$$\begin{cases} \dot{\eta} = \dot{\eta}_0(p_0 - p) & \text{if } p < p_0, \\ \dot{\eta} = 0 & \text{if } p \geq p_0, \end{cases} \quad (12)$$

where p_0 is the threshold pressure for damage growth and η_0 is a material constant.

A linear equation of state was adopted for these material in the form:

$$p = K \left(\frac{\rho}{\rho_0} - 1 \right), \quad (13)$$

K being the bulk modulus of the ceramic material, ρ its density and ρ_0 its reference density. Table 3 shows the parameters adopted for these ceramic materials.

3.2. Erosion criteria

One of the most important aspects in the numerical simulation of ballistic impacts is the erosion criteria for the materials. This not only drives the removal of distorted zones of the mesh but also allows a simulation of target erosion. Here the instantaneous effective geometric strain $\bar{\epsilon}_{crit}$ was adopted as the erosion parameter. Since the critical value of this strain greatly affects the simulation, it was previously tuned for each material by comparing experimental and numerical results of different Depth of Penetration tests. Eight preliminary impacts were performed onto $10 \times 10 \times 10 \text{ cm}^3$ aluminium blocks with and without an 8.3 mm thick ceramic tile bonded on it

Table 4
Critical values for the erosion criteria

Material	ϵ_{crit}
Aluminium	1
Epoxy	1.5
Alumina	3
Tungsten carbide	4

with a 0.4 mm adhesive layer. All these materials, and the projectile, were those used for the experimental work. The penetration data were measured with an ultrasonic device. Experimental mean values plus and minus standard deviation for the reference penetration (uncovered block) and for the residual penetration (covered block) were respectively 42.0 ± 1.0 mm and 20.0 ± 0.5 mm. The critical values of $\bar{\epsilon}_{\text{crit}}$ (Table 4) were fixed to fit the penetration depth on the metallic block.

3.3. Grids

A Lagrangian axisymmetric mesh of around 10,000 nodes was used for all the solids: projectile, ceramic tile, adhesive layer and backing plate. Of each configuration, 12 different adhesive thickness were studied, from 0.1 to 1.1 mm with an increment of 0.1 mm. Mesh density was refined close to the symmetry axis.

4. Results

From both the experimental test and the numerical simulations it was clear that in configuration I, the armour produced projectile arrest (region A of Fig. 3) for all the thicknesses of adhesive. Configuration II showed cases of arrest and also of perforation. For a better understanding of the influence of the adhesive thickness, the following variables were analysed:

Shear strain in the adhesive layer.

Damage in the ceramic tile.

Aluminium backing plate deformation.

Remaining armour thickness (when projectile arrest).

Projectile residual velocity (when perforation).

For an analysis of these variables by numerical simulation, the nodes shown in Fig. 7 were considered.

4.1. Shear strain in the adhesive layer

In the course of penetration, ceramic fragments were dispersed radially from the path of the projectile, producing shear strains γ_{rz} (see Fig. 7 for axes orientation) in the material up to

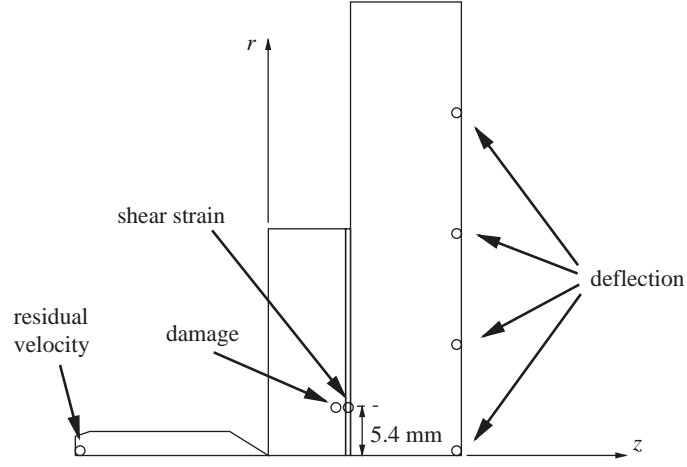


Fig. 7. Position of the nodes choose for the measurement of the analysed variables.

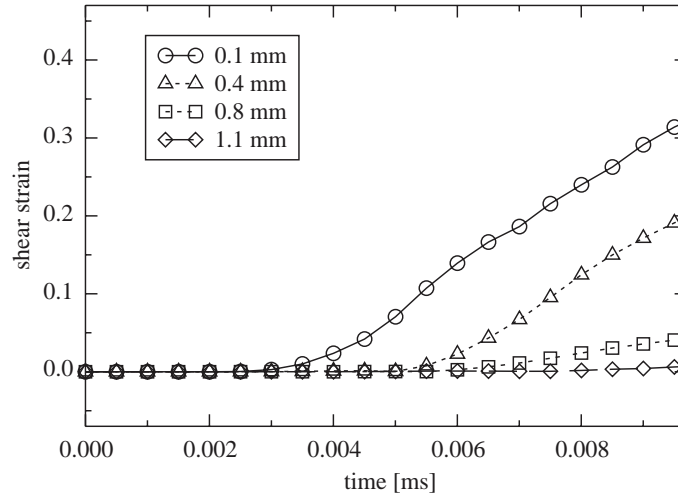


Fig. 8. Shear strain time history in the adhesive for different adhesive layer thicknesses for configuration I.

fracture. The effect of the thickness of the adhesive on the strain rate is expressed by

$$\dot{\gamma}_{rz} = \frac{v_c - v_b}{h_a}, \quad (14)$$

where v_c and v_b are the radial velocities at the points of the ceramic and backing plate in contact with the adhesive layer, and h_a the adhesive layer thickness, so low values of h_a lead mean higher shear strain rates. Figs. 8 and 9 show the temporal evolution of this deformation at a distance of 5.4 mm from the axis of symmetry for the two configurations alumina/aluminium. The thinner layers of adhesive were seen to induce larger shear strains followed by premature failure and easy removal of the ceramic tile. This was confirmed experimentally (Fig. 10): in most of the armours with the thinnest layer of adhesive the ceramic tile was completely removed after impact, whereas

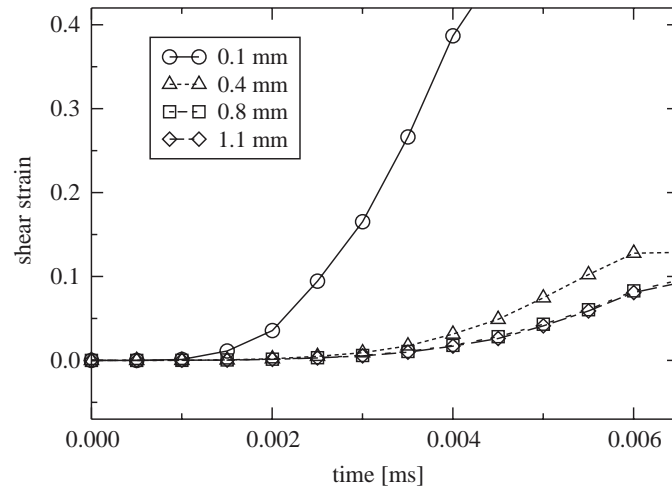


Fig. 9. Shear strain time history in the adhesive for different adhesive layer thicknesses for configuration II.



Fig. 10. Comparison of the remaining ceramic tile after impact for an epoxy adhesive layer of thicknesses of 0.1 mm (left) and 1.1 mm (right).

some pieces remained attached to the backing plate when the thicker layer was used. This could be of importance in later impacts, affecting the multi-hit capability of the armour.

4.2. Damage in the ceramic tile

One of the most important stages of the impact process in terms of efficiency of the ceramic tile is the initial phase immediately after contact with the projectile [9,10]. During the first

microseconds of the impact event, conical cracks propagate from the border of the contact zone. Fragmentation of the ceramic at the rear of the tile begins when the elastic compression wave has travelled through the whole thickness; when this wave reaches the ceramic/adhesive interface, bending of the tile generates circumferential tensile stresses and radial cracks propagate backwards (Fig. 11). Thus, this fragmentation process is prevented when a stiff layer is placed behind the ceramic tile [5]. The duration, t^* , of this process [10] may be calculated from

$$t^* = \frac{6h_c}{u_c}, \quad (15)$$

in which h_c stands for the thickness of the tile and u_c the speed of propagation of the elastic waves. In our analysis, the order of magnitude of t^* is a microsecond. Figs. 12 and 13 illustrate the temporal evolution of damage in the rear of the ceramic tile along the axis of symmetry in the two alumina/aluminium configurations. Fragmentation is notably influenced by the thickness of the adhesive in the first microseconds, the more so in the thickest layers. Bending of the rear face of the ceramic tile, which causes its radial cracking, is lesser with thinner layers of adhesive because

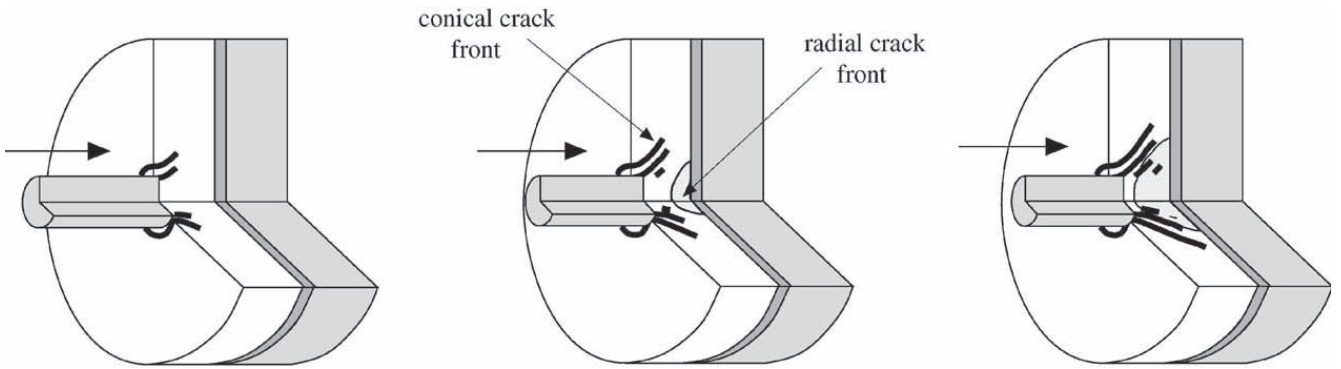


Fig. 11. Ceramic fragmentation process.

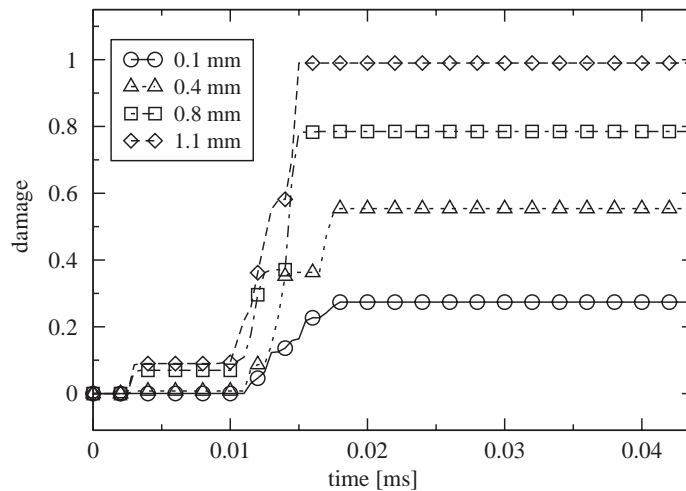


Fig. 12. Ceramic damage time history for different adhesive layer thicknesses for configuration I.

the more rigid metal plate is closer to the tile. In fact, damage is hardly perceptible when the layer of resin is 0.1 mm. This lesser damage in the ceramic tile at the initial stage of fragmentation checks the penetration for the projectile and raises the degree of protection.

4.3. Aluminium backing plate deformation

The efficiency of the metallic plate may be estimated from the degree of its plastic deformation after impact. This is a notable mechanism of the absorption of the kinetic energy of the projectile during penetration: the larger the area affected and the greater the distortion of the rear panel, the greater the dissipation of energy. The fire test of configuration I showed that the deformation of

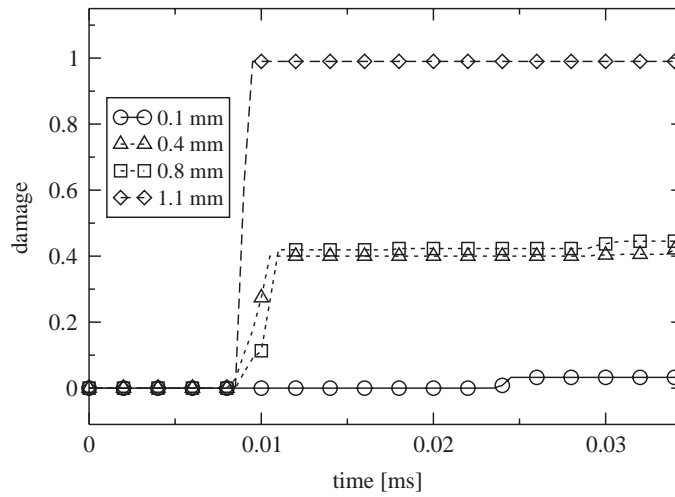


Fig. 13. Ceramic damage time history for different adhesive layer thicknesses for configuration II.

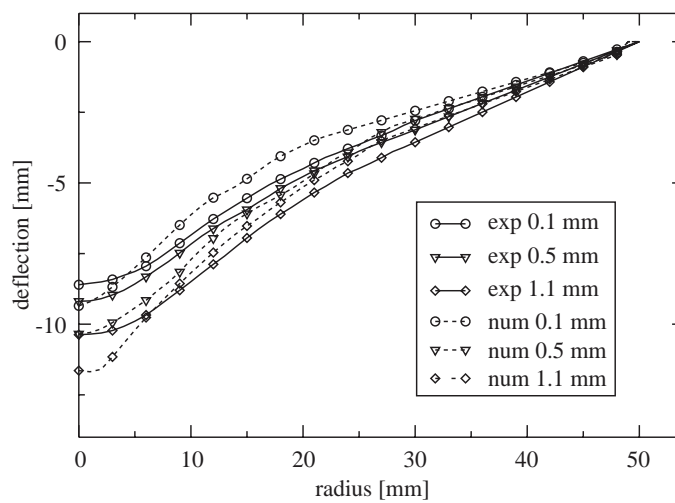


Fig. 14. Final backing plate deformation for different adhesive layer thickness. Numerical and experimental results. Standard deviation of the experimental values lower than 0.3 mm.

the backing plate increases with the thickness of the adhesive (see the curves in Fig. 14), and the same trend is apparent in the result of the simulations. The numerical analysis showed that with thicker layers of adhesive, the energy of the projectile, distributed over a wider area of the aluminium plate (Fig. 15), gives rise to a greater deformation. Hence this absorption of energy improves the quality of protection. No similar analysis was possible for configuration II: so many perforations were obtained that measurements of deformation were ruled out.

4.4. Remaining armour thickness and residual velocity of projectile

To establish a connection between the thickness of the adhesive layer and the efficacy of the protection, a study must be made of the variables involved in the whole response to impact. The

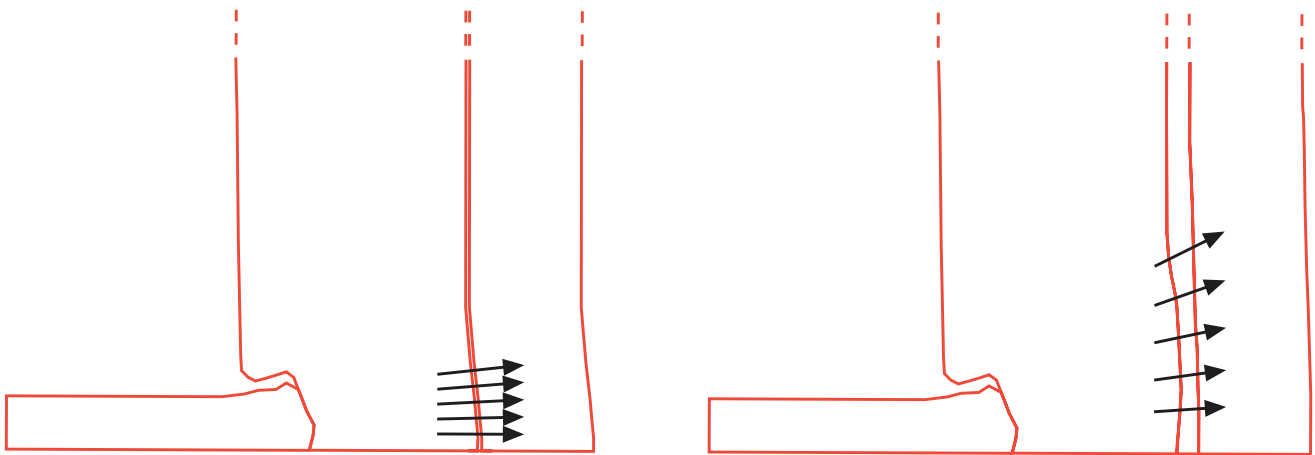


Fig. 15. Influence of the adhesive layer thickness on the extension of the load transmission zone. Thin layer (left), thick layer (right).

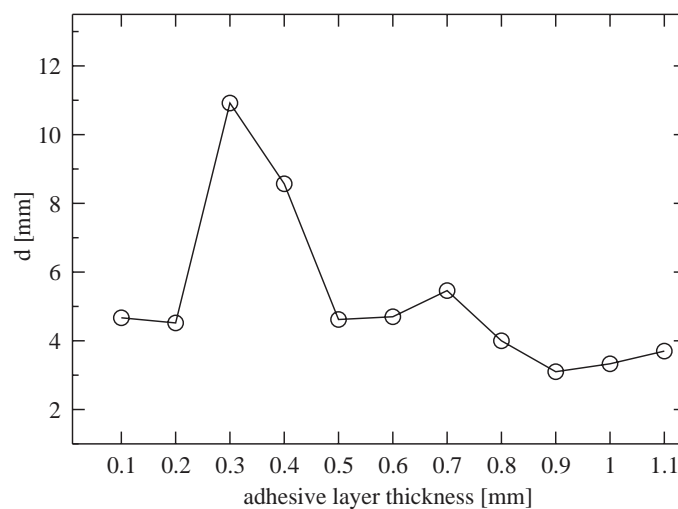


Fig. 16. Remaining armour thickness d versus adhesive thickness for configuration I.

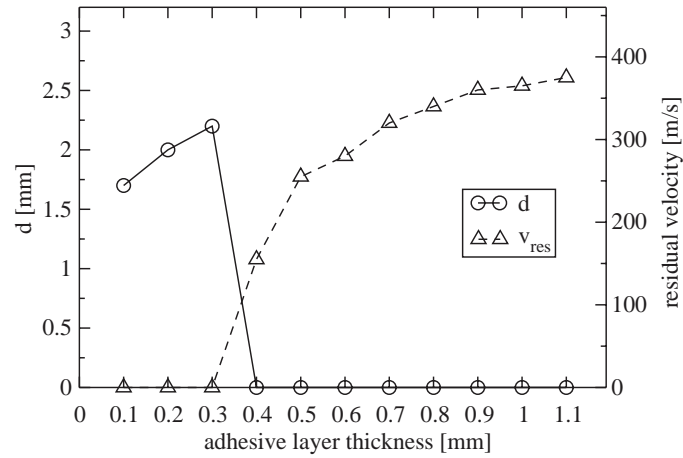


Fig. 17. Remaining armour thickness d and projectile residual velocity versus adhesive thickness for configuration II.

numerical analysis of configuration I showed that the best protection is achieved with a thickness of the adhesive of 0.3 mm (Fig. 16). The same is true of the data of configuration II which has examples of arrest and of penetration (Fig. 17). As mentioned above, the thickness of the adhesive has a contrary effect on the efficacy of protection in terms of the variables *ceramic damage* and *backing plate deformation*: a thin layer of resin hinders the fragmentation of the ceramic by reduces the zone of the backing plate that helps to absorb energy. These opposing trends justify the appearance of the optimum according to our observations.

5. Conclusions

The study of the influence of the adhesive layer thickness on the efficiency of lightweight ceramic armours, analysed by experimental testing and numerical simulation, showed that the efficacy of the armour is affected by three different effects related to the adhesive thickness: *shear stress* on the adhesive decreases with a thick layer, avoiding its failure and holding the ceramic material attached to the backing plate after impact, *ceramic spalling* is reduced with thin adhesive layers that prevent bending of the hard tile and *energy absorption* by the backing plate is greater with a thick layer, which facilitates load transfer from ceramic to metal. Therefore a variation of the thickness of the adhesive layer affects the efficiency of the armour and a value of 0.3 mm was found optimum for every alumina/aluminium configuration considered.

Acknowledgements

The authors are indebted to the Dirección General de Enseñanza Superior (DGES) for the financial support of this work (Project PB-0380). Although the project finished several years ago, it motivated the initiation of this work.

References

- [1] Ogorkiewicz RM. Development of lightweight armour systems. In: Proceedings of lightweight armour system symposium. Cranfield, England; 1995.
- [2] Zukas JA, Nicholas T, Swift HF, Greszczuk LB, Curran DR. Impact dynamics. New York, USA: Wiley; 1992.
- [3] Marshall J. Composite ballistic armour. In: Proceedings of the first international conference on composites engineering, ICCE/1, New Orleans; 1994.
- [4] James B. Modification of ceramic failure in impact by stress wave management. In: Proceedings of lightweight armour system symposium, Cranfield, England; 1995.
- [5] Zaera R, Sánchez-Sáez S, Pérez-Castellanos JL, Navarro C. Modelling of the adhesive layer in mixed ceramic/metal armours subjected to impact, Composites: Part A, vol. 31. 2000; p. 823–33.
- [6] Century Dynamics Inc., Autodyn-2d v4.1 users manual. PhD thesis, San Ramon CA, USA; 1997.
- [7] Steinberg DJ, Cochran SG, Guinan MW. Constitutive model for metals applicable at high strain rate. J Appl Phys 1980;51(3):1498–504.
- [8] Cortés R, Navarro C, Martínez MA, Rodríguez J, Sánchez-Gálvez V. Numerical modelling of normal impact on ceramic composite armours. Int J Impact Eng 1992;12:639–51.
- [9] Zaera R, Sánchez-Gálvez V. Analytical modelling of normal and oblique ballistic impact on ceramic/metal lightweight armours. Int J Impact Eng 1998;21(3):133–48.
- [10] den Reijer PC. Impact on ceramic faced armours. PhD thesis, Delft University of Technology, 1991.
- [11] Roberson CJ. Ceramic materials and their use in lightweight armour systems. In: Proceedings of lightweight armour system symposium, Cranfield, England; 1995.